

Proceedings of 7th Transport Research Arena TRA 2018, April 16-19, 2018, Vienna, Austria

LiNi_{0.5}Mn_{1.5}O₄ cathode materials for high-voltage, next-generation automotive Li-ion cells

D. Zarvalis^{a*}, G. Ganas^a, G. Kastrinaki^a, G. Karagiannakis^a, A.G. Konstandopoulos^{a, b},
A. Eguia-Barrio^c, M. Bengoechea^c, I. de Meatza^c, A. Ahniyaz^d, D. Peralta^e, P.
Michallone^e

^a Aerosol & Particle Technology Laboratory, CErTH/CPeRI, P.O. Box 60361, 57001, Thessaloniki, Greece

^b Department of Chemical Engineering, Aristotle University, P.O. Box 1517, 54006, Thessaloniki, Greece

^c IK4-CIDETEC, Parque Científico y Tecnológico de Gipuzkoa, Paseo Miramón 196, 20014, Donostia-San Sebastián, Spain

^d Chemistry and Materials and Surface Unit, RISE Bioscience and Materials Division, RISE Research Institutes of Sweden, Drottning Kristinas väg 45, P.O.Box 5607, SE-11486, Stockholm, Sweden

^e Commissariat à l'Energie Atomique et aux Energies Alternatives, Laboratoire des Composants pour Batteries, CEA – LITEN, 17, rue des Martyrs, 38054 Grenoble, France

Abstract

The insufficient autonomy of Electric Vehicles (EVs), which is mainly due to the limited energy density of automotive batteries, can be addressed by increasing the specific energy and/or the average operating voltage of the active cell materials. LiMn_{1.5}Ni_{0.5}O₄ (LNMO) is a top candidate active cathode material due to its access to a rare two-electron transition from Ni²⁺ to Ni⁴⁺ at two voltage plateaus near 4.7 V vs. Li⁺/Li, a theoretical capacity of 147 mAhg⁻¹ and fast three-dimensional Li-ion diffusion paths within the cubic lattice. Furthermore, LNMO is a relatively low-cost material with fairly good charging rate capability, suitable for EV requirements. However, the employment of LNMO in next-generation Li-ion batteries is prohibited by phenomena related to structural stability due to manganese dissolution and electrolyte compatibility. Structural modification via the inclusion of suitable dopants and proper surface treatment constitute promising solutions to these problems. Materials development for more efficient automotive batteries is an urgent task. In this work, four research organizations have joined efforts to realize LNMO cathodes appropriate for EVs. Three partners in this team worked on the materials development, and the fourth partner worked on the benchmarking of the materials. We have exploited nine different synthesis technologies for the pristine LNMO. From the evaluated technologies, three have been identified as most promising and were optimized for the specific application: the co-precipitation, the sol-gel and the aerosol spray pyrolysis methods. Several calcination profile conditions of the produced powder were studied obtaining two LNMO spinel phases: the ordered (*P4₃32*) and the disordered (*Fd-3m*) with the latter identified as the most electrochemically active. Five dopants have been introduced into the most promising LNMO lattices with Fe and Al proven to be the best-performing ones. Twelve materials have been considered for the LNMO particle surface treatment, and the Al₂O₃ was evaluated as the one showing satisfactory cyclic stability. We have used Scanning and Transition Electron Microscopy (SEM/TEM), micro-Raman spectroscopy, X-Ray Powder Diffraction (XRD) and Particle Size Analysis (PSD) for the structural characterization of the products. The most promising compositions have been scaled up to quantities sufficient for the manufacture of battery cells used in the automotive sector. In this work, we will present the most significant results from the above developments including results from electrochemical performance tests of electrodes in half and full coin cells (HCC/FCC). At HCC and C/5 we managed to obtain a specific capacity of more than 130 mAh/g with about 10% irreversible capacity loss. In FCC (vs. graphite) and C/20 we have obtained materials with 118 mAh/g specific capacity and about 20 % irreversible loss. During cycling of FCCs at 1C, with the best performing material, we have attained about 80 % of the initial capacity after 100 charging/discharging cycles. Future developments should focus on increasing the cycling ability of the full-cell by optimising the active materials (both cathode and anode), the electrolyte as well as the electrode structure.

Keywords: Next generation Li-ion batteries, High-voltage cathode materials, LNMO cathodes

Nomenclature

ASP	Aerosol Spray Pyrolysis
EC	Ethyl Carbonate
EDS	Energy Dispersion Spectroscopy
EELS	Electron Energy Loss Spectroscopy
EMC	Ethyl Methyl Carbonate
EV	Electric Vehicle
FCC	Full Coin Cell
FE-SEM	Field Emission Spectroscopy
HCC	Half Coin Cell
HR-TEM	High-Resolution Transmission Electron Microscopy
LNMO	$\text{LiNi}_{0.5}\text{Mn}_{1.5}\text{O}_4$
NMP	N-methyl-2-Pyrrolidone
PSD	Particle Size Distribution
PVdF	Poly-Vinylidene Fluoride
SEM	Scanning Electron Microscopy
TEM	Transmission Electron Microscopy
XPS	X-ray Photoelectron Spectrometer
XRD	X-ray Diffraction

1. Introduction

The development of next-generation Li-ion battery technology with improved lifespan, energy and power density is one of the most important challenges for the implementation and wider commercialisation of electric vehicles. Towards this, research is ongoing for the development of suitable cathode materials as well as compatible electrolytes. A large number of cathode materials has been explored extensively such as layered LiMO_2 (Reddy et al., 2011) olivine LiMPO_4 (Miao et al., 2014) and spinel LiM_2O_4 . One promising material of the latter structure is $\text{LiNi}_{0.5}\text{Mn}_{1.5}\text{O}_4$ (LNMO) due to its high charge/discharge potential (~ 4.7 V vs Li/Li^+), good theoretical specific capacity (~ 147 mAh/g) (Patoux et al., 2009), and its environmental friendliness (Liu et al., 2014). The European H2020 project titled eCAIMAN, “Electrolyte, Cathode and Anode Improvements for Market-near Next-generation Lithium Ion Batteries” (project reference 65331), seeks to utilise LNMO-based cathode materials for the production of next-generation Lithium-ion cells. Within the project, different possibilities for the synthesis of LNMO have been examined as well as several approaches have been followed to address problems arising from the incorporation of such materials as active cathodes.

LNMO appears in two different space groups, namely the ordered single cubic $P4_332$ and the disordered face-centred $Fd-3m$ structure. In the $P4_332$ case, Mn^{4+} and Ni^{2+} ions are located in $12d$ and $4a$ sites respectively, with the absence of Mn^{3+} ions, while Li ions exist at $8c$ sites and O at $8c$ and $24e$ sites. In the $Fd-3m$ case, Mn^{4+} and Ni^{2+} ions are randomly distributed at $16c$ sites of the lattice, while Li and O are located at $8a$ and $32e$ sites respectively (Oh et al., 2009). Unlike the $P4_332$ structure which exhibits a stoichiometric amount of oxygen atoms, the disordered $Fd-3m$ demonstrates oxygen vacancies, δ , thus leading to a $\text{LiNi}_{0.5}\text{Mn}_{1.5}\text{O}_{4-\delta}$ structure with certain Mn ions being reduced to Mn^{3+} to maintain the charge balance (Kim et al., 2009).

Despite its advantages, LNMO may exhibit a significant reduction in capacity during cycling due to Mn diffusion in the mass of the electrolyte caused by various lattice modifications accompanied by the Jahn-Teller effect (Pieczonka et al., 2013). Studies have shown that the LNMO synthesis method does not only affect morphology, particle size and crystallinity, but also plays a key role in stoichiometry, crystal structure, impurities, and thus the electrochemical performance (Wang et al., 2016). Numerous synthesis methods such as solid-state (Zheng et al., 2012; Zhu et al., 2013), co-precipitation (Gu et al., 2015; Feng et al., 2013), sol-gel (Lin et al., 2014), molten salt (Wen et al., 2006; Liu et al., 2014), emulsion drying (Myung et al., 2002; Lee et al., 2002) and hydrothermal route (Xue et al., 2014) are presented in the literature. Relevant review papers (Kraytsberg et al., 2012; Potapenko et al.,

2014; Wang et al., 2015; Myung et al., 2015; Yi et al., 2016; Xu et al., 2017) demonstrate the electrochemical performance of differently synthesised LNMO materials. However, these results are not easily comparable since performance, at the cell level, depends on many parameters (electrolyte, electrode formulation, cell design, charging/discharging method, etc.), which vary among the different research groups. As a consequence, it's hard to formulate concrete conclusions on the applicability of LNMO materials for the next generation Li-ion automotive battery.

In eCAIMAN project, we have exploited nine different synthesis technologies for the synthesis of LNMO. The most promising ones are presented in more detail in this work. The produced by different methods materials have been characterized following the same pre-determined procedures concerning particle composition, structure and size as well as their electrochemical performance at half and full-cells.

2. Characterisation methodology

The X-ray Diffraction (XRD) technique (Siemens D500/501 X-ray Diffractometer with Cu K α radiation (5°-80° at a scan rate of 0.040°/s) was used for the identification of the LNMO structures. However, the contrast observed between the XRD spectra of the ordered $P4_332$ and disordered $Fd-3m$ LNMO space groups was relatively poor, and therefore the distinction of the two was facilitated by Raman spectroscopy (micro-Raman Spectrometer, Renishaw inVia Reflex). According to Amdouni et al. (2006), more peaks are expected to appear in $P4_332$ than in $Fd-3m$ case. Specifically, in both space groups, a peak of high intensity appears at a wavenumber of $\sim 636\text{ cm}^{-1}$ which corresponds to the symmetrical Mn-O bond vibration of the MnO_6 octahedra, while an extra peak is expected at $\sim 490\text{ cm}^{-1}$, which can be attributed to the Ni^{2+} -O lattice bond vibration. In $P4_332$ space group, an additional peak at $\sim 400\text{ cm}^{-1}$ (Ni^{2+} -O bonds) is expected along with additional peaks at 220 cm^{-1} , 240 cm^{-1} and a double peak at 590 cm^{-1} , suggesting the well-dispersed positions of Ni and Mn in the lattice due to reduced symmetry of the $P4_332$ structure.

XPS spectra were recorded by facilitating an X-ray Photoelectron Spectrometer (Kratos AXIS Ultra^{DLD}, Kratos Analytical), using a monochromatic Al X-ray source. The analysis area was $<1\text{ mm}^2$, with most of the signal from an area of $700 \times 300\text{ }\mu\text{m}$.

The morphology of the prepared samples was studied by Scanning Electron Microscopy (SEM) and high-resolution Transmission Electron Microscopy (TEM) techniques using a JEOL JSM-6300 scanning microscope and a JEOL JEM 2010 high-resolution transmission microscope respectively. Aerodynamic Particle Size Distribution (PSD) analysis was performed using a TSI PSD 3603 Particle Size Distribution Analyzer. The specific surface area was calculated through Brunauer-Emmett-Teller (BET) method using N_2 adsorption porosimetry (Micrometrics ASAP 2000, at 77K, after degassing the samples at $250\text{ }^\circ\text{C}$), while the tapped density of the resulted materials was calculated through a tap density analyser (Quantachrome Instruments).

The electrochemical performance of synthesised LNMO was evaluated at the laboratory scale by assembling both half-coin (HCC) and full-coin cells (FCC). During the preparation of the cathode, an N-methyl-2-pyrrolidone (NMP) slurry was prepared, consisting of 80 wt % of active material with the rest 20 wt% being carbon black (C65) and Poly-Vinylidene Fluoride (PVdF) as electronic conduction enhancer and binder, respectively. After coating the slurry on an aluminium foil using the doctor blade technique, the resulted electrodes were dried under vacuum, and the coin cell assembly followed. In HCC pure Li was used as anode while in FCC an in-house developed graphite-based anode was used. In both HCC and FCC tests, customised electrolytes were utilised. The cells were tested in a potential window of 3.5-5V at room temperature in a working C-rate range between C/5 (5 h) and 5C (12 min). C-rate calculations were made based on a LNMO specific capacity of 135 mAh/g .

3. Synthesis methods

In total, nine synthesis techniques have been employed. These were the following: Aerosol Spray Pyrolysis (ASP), Co-precipitation, Solid mixing, Solid State Reaction with Spray drying, Sol-Gel, Polymer assisted, Micro-emulsion, Liquid Oxalate route – acetates and Polymer assisted. The synthesised products were further treated with many different methods concerning calcination and application of protective coatings. As a result, a significant number of final materials was realized. Preliminary evaluation tests and characterisation revealed the most promising ones. From the most promising methodologies, the selected top-three ones are presented in more detail in the following sections. The first one concerns an ASP synthesised doped LNMO without coating. The

second material presented is again without coating and is synthesised via a two-step method based on coprecipitation combined with solid mixing. The third material is pristine LNMO coated with a protective layer. The pristine material is synthesised via solid mixing and subsequent calcination, and the coating is applied via mixing of an aqueous solution of the LNMO with a solution containing precursor materials of the coating.

3.1. Aerosol Spray Pyrolysis (ASP)

ASP is a one-step aerosol process where a precursor solution is atomised into fine droplets that are in-situ calcined when entering a tubular reactor (Lorentzou et al., 2009; Lorentzou et al., 2011). Every droplet is a micro-reactor that undergoes evaporation of the solvent and precipitation of reactants when exposed to different temperature profiles and forms a single particle which is trapped in a filter at the reactor exit. The chemistry of the precursor solution, as well as the ASP process parameters (e.g. temperature profile, aerosol flow, gas type), can control the particle synthesis at the molecular level (bottom-up synthesis) thus leading to various particle morphologies. The precursor solution chemistry was standardised via liquid-based synthesis before proceeding to the ASP method, while post-calcination was also applied to retrieve the LNMO spinel. Through different post-calcination profiles, it has been established that temperatures above 700°C lead to the *Fd-3m* while low temperature lead the LNMO to be crystallized to the *P4₃32* space group.

3.2. Two-step synthesis: Coprecipitation and solid state

Initially, solutions of precursor materials (sulphates and carbonates of Ni, Mn, Na and Al) are continuously injected in a stirring tank reactor. After controlling parameters such as pH, feeding flow, temperature, blade geometry and stirring speed, large spherical aggregates of $\text{Ni}_{0.2222}\text{Mn}_{0.7407}\text{Al}_{0.0247}\text{CO}_3$ were formed. As a second step, the carbonate precursor was mixed with a Li source (Li_2CO_3) and the mixture was calcined at elevated temperature to obtain Al-LNMO aggregates of spherical morphology.

3.3. Solid state synthesis and application of coating

LNMO was synthesised according to the protocol reported by Kohs et al.. Namely, a stoichiometric mixture ($\text{LiNi}_{0.5}\text{Mn}_{1.5}\text{O}_4$) of metal carbonate salts (Li_2CO_3 , NiCO_3 and MnCO_3) was mixed for about 10 min and calcined at 450°C for 1h and then at 850°C for 18 h (heating rate 3°C min⁻¹) to obtain pristine LNMO powders. For the FePO_4 coating, a 2.8 wt% LNMO water dispersion was prepared by mixing 6.79 g of pristine LNMO with 244.67 g of water and stirring overnight. In order to improve the dispersion of the LNMO particles further, the dispersion was sonicated (ultrasonic cleaner USC-THD) for 90 min. Laser diffraction analysis measurements indicated that the particle size of the resultant water dispersion pristine LNMO was around 5 µm (D50). Afterwards, a suitable amount of diluted aqueous solution of $(\text{NH}_4)_2\text{HPO}_4$ and $\text{Fe}(\text{NO}_3)_3$ was added dropwise to the mixture under stirring to obtain 3 wt% FePO_4 -coated LNMO. Consequently, FePO_4 was formed and deposited onto the surface of the LNMO particles. After repeated rinsing and filtering at 5000 rpm for 5 min, the cake was first dried at 120°C for 12 h and then heated at 400°C for 6 h. Finally, a 3 wt% FePO_4 -coated LNMO powder was obtained. Results and discussion.

4. Results

4.1. Doped LNMO from ASP

Besides chemistry, the concentration of active precursors in the solution can affect the morphology of the produced particles. We have studied concentrations in the range of 0.1-3M. Fig. 1 presents the as-produced and the calcined (800°C) materials from 0.1 and 1 M solutions. The smaller the concentration is, the more porous the as-produced material is. The as-produced material from 0.1 M solution has a core-cell structure with the core being mostly empty. Calcination leads to the collapse of the previous structures with the formation of primary particles which aggregate in near-spherical structures. Again the concentration of 0.1M leads to very porous spheres with the core being mostly empty. The concentration of 1 M leads to substantially denser particles with better electrochemical activity, as proved from preliminary electrochemical characterisation. High particle porosity has an adverse effect on the material density and consequently the cell energy capacity. High porosity could also have a negative effect on electronic conductivity. Increasing the concentration from 1M to 3M had no further significant effect on particle morphology.

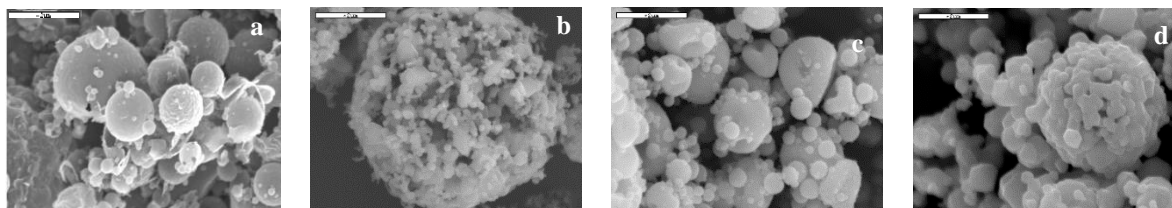


Fig. 1 SEM pictures of ASP synthesised LNMO: (a) As produced material from 0.1M solution (b) Calcined material from 0.1M solution (c) As produced material from 1M solution (d) Calcined material from 1M solution.

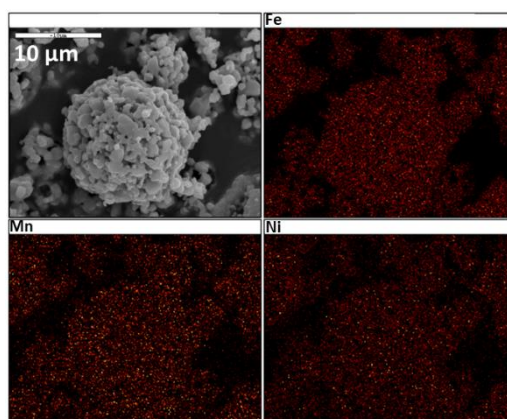


Fig. 2 Left: SEM picture and EDS mapping of ASP synthesised Fe-doped LNMO. Right: Specific discharge capacity of two different samples of Fe-doped LNMO.

As a next step, we investigated the calcination profile that would maximise performance. Several calcination profiles have been studied, also considering relevant previous studies (Song et al., 2012; Takahashi et al., 2004; Pasero et al., 2008;). One-step or two-step (calcination at one temperature and then an additional calcination at a lower temperature) processes have been considered. The two-step processes did not bring any special advantage with concern to the specific energy capacity. The ordered LNMO phase does not have good electrochemical performance compared to the disordered one. The highest activity was exhibited with calcination temperatures of 800 °C.

Three dopants were used for the ASP synthesised LNMO: Al, Mg and Fe. The size and morphology of the materials did not differentiate with the different dopants employed. Fig. 2 presents the SEM picture and the mapping of the Fe, Mn and Ni elements showing the homogeneous distribution of the metal ions within the material structure. The Fe-LNMO demonstrated the best electrochemical performance among the ASP synthesised samples.

4.2. Doped LNMO from coprecipitation and solid state synthesis

In coprecipitation, primary particles with small diameter are aggregated in large and spherical secondary particles. The synthesis process was first optimized for the $\text{LiNi}_{0.5}\text{Mn}_{1.5}\text{O}_4$ material formula. Both hydroxide and carbonate routes of synthesis were evaluated. In all cases, spherical secondary particles are recovered, one of the main difference in terms of morphology is the shape of the primary particles. Carbonate route leads to small cuboidal primary particles and the hydroxide route leads to flake-shaped particles. At the end, materials obtained with carbonate route had better performances.

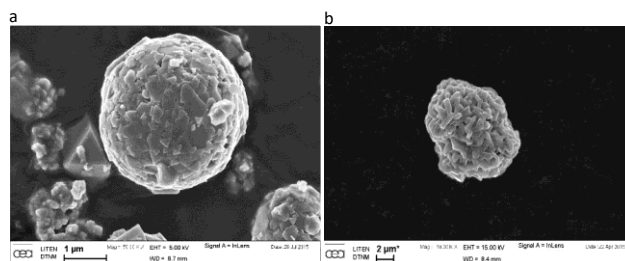


Fig. 3 SEM pictures of (a) LNMO obtained with carbonate synthesis and (b) LNMO obtained with hydroxide synthesis.

Then the calcination temperature of the solid state synthesis was optimized in order to maximize the material density. We observed that the primary particles grow and the porosity of the secondary particles decreases when the temperature increases. For temperature higher than 1000°C, the size of the primary particles become too big and the spherical shape of the secondary particles cannot be conserved (fig. 4).

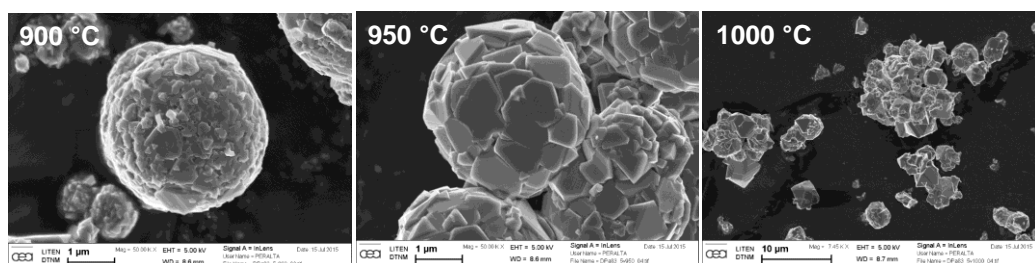


Fig. 4 Influence of the calcination temperature on the LNMO morphology

As a next step, a low amount of aluminum is added during the coprecipitation process in order to improve the electrochemical performances of our material. We obtained a LNMO with the following formula: $\text{LiNi}_{0.495}\text{Mn}_{1.495}\text{Al}_{0.01}\text{O}_4$. The material crystallizes in the Fd-3m space group and the spherical morphology of the particles is maintained when aluminum is added during the synthesis (fig.5).

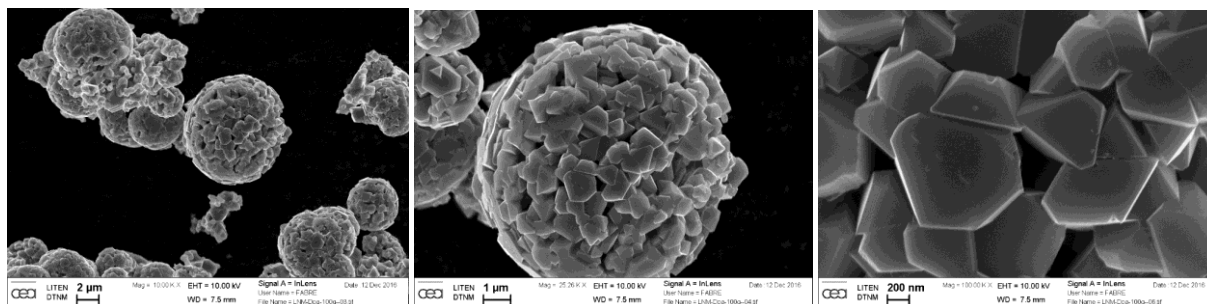


Fig. 5 SEM pictures of Al-doped LNMO synthesised by co-precipitation / solid state method.

4.3. Coated LNMO

The solid mixing of precursor materials and further calcination resulted in well-crystalline materials consisting of large amorphous aggregates of LNMO crystals (Fig 6.). In this case, no spherical particles were shaped, and there are no significant differences in the pictures from the coated and uncoated materials. To examine the homogeneity of the coating, both HR-TEM and EELS were performed for 3.0wt% FePO_4 -coated LNMO sample (Fig. 7). TEM study indicated the presence of a very thin layer of amorphous coating layer (~30 nm) on the surface of well-crystalline LNMO particles. Some facets of LNMO particle were not covered by FePO_4 completely, indicating the inhomogeneity of FePO_4 coating. Observing the composite EELS image it is clear that FePO_4 coating is mainly distributed on the surface of the LNMO particles as well as small amounts of free FePO_4 are also present.

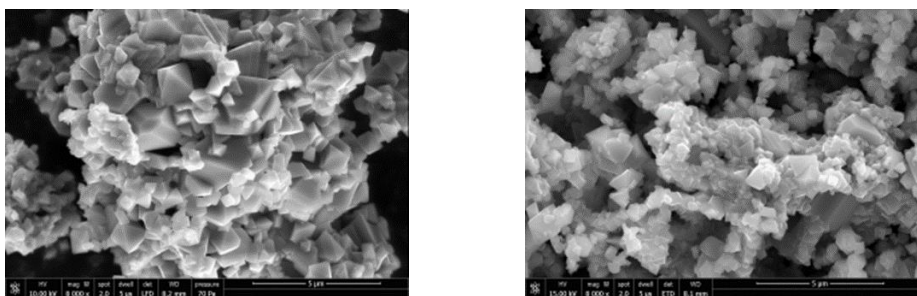


Fig. 6 SEM pictures of uncoated (left) and coated LNMO particles.

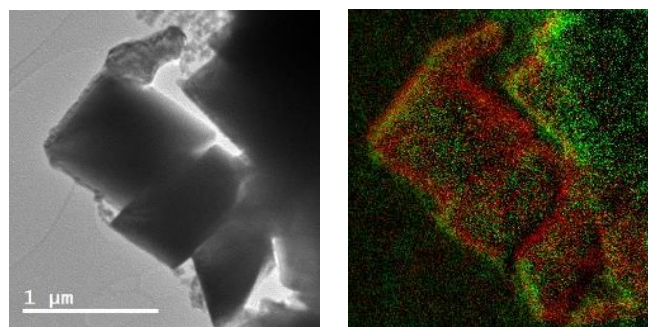


Fig. 7. TEM picture (left) and EELS mapping (right) of FePO₄-coated LNMO particles, coated with 3.0wt% FePO₄ (overlay: Red: Fe, Green: Mn)

XPS analysis result of the FePO₄ coated LNMO powder is shown in Table 1. XPS data indicated the presence of both phosphor and Fe at the outmost surface layer (2-10nm) of LNMO and very low amount of Ni and Mn indicating a successful FePO₄ coating of LNMO particles. However, the presence of small amount of Ni and Mn also shows that presence of uncoated region also on the LNMO particles.

Table 1. Quantitate analysis of elements at the 2-10nm surface of LNMO

Sample	Atomic %											
	Mg	Na	Ni	Fe	F	Mn	O	N	C	S	P	Al
FePO ₄ coated LNMO	-	-	1.5	5.8	1.6	7.6	61.5	(0.2)	13.7	0.3	7.8	-

4.4. Electrode processing evaluation and electrochemical performance comparison

Most promising active material samples were selected to carry out slurry and electrode engineering assessment towards the upscale of 5V LNMO/Graphite prototype cells. Electrode slurry mixing and coating process was evaluated for the two doped samples (Al-LNMO and Fe-LNMO) and the coated (LNMO/FePO₄) one for a fixed formulation LNMO/C65/PVdF = 80/10/10 on 50g-solids slurry batch. The electrode formulation and slurry mixing process, based on pre-dispersion of the C65 carbon black in the PVdF/LNMO solution, were selected after optimization procedures to achieve homogeneous and stable slurries and manufacture technical electrodes (target loading 1.6mAh/cm², ca. 13-14mg/cm²) with efficient dispersion of the 10% carbon black necessary for electrical conductivity of these samples.

Rheological measurements of the cathode slurries prepared for the three active materials (Fig. 8) showed appropriate shear thinning behaviour and stability at rest for good coating quality within the viscosity range of 10-20 Pa·s at 10s⁻¹ targeted in a coating line. The coated sample (LNMO/FePO₄) with non-spherical particles and of higher particle size presented slightly less stability (change in slope observed below 0.2s⁻¹) while the nano-structured Fe-LNMO required higher solvent volume leading to lower viscosity. These slurries were coated onto 20μm-thick battery grade Aluminum foils by lab-scale doctor-blade (automatic film applicator) using a wet gap of 500-600μm to achieve the loading target of ca. 1.6mAh/cm² for all samples.

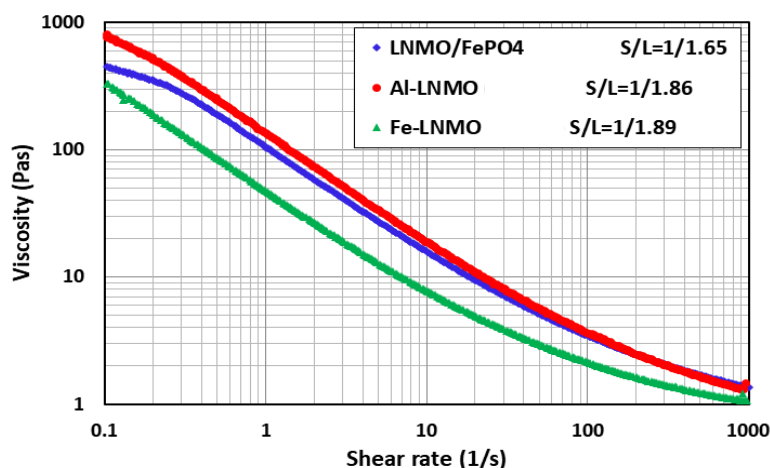
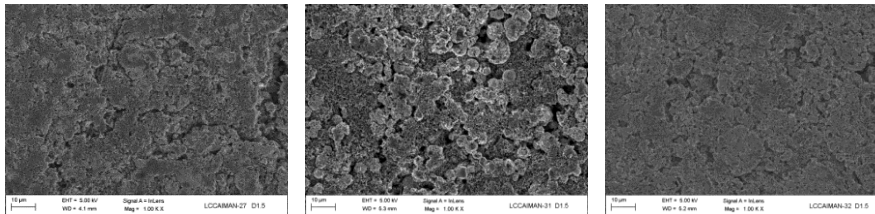


Fig. 8 Rheology of electrode slurries with formulation [LNMO/C65/PVdF = 80/10/10] and 34-37% solids (Solid-to-liquid ratio, S/L, provided in the legend).

Table 2 summarizes density, morphology (FE-SEM) and adhesion (measured on 90° peel test) obtained after calendaring the electrodes to 1.5g/cm³ (50% thickness reduction limitation without electrode bending) in order to decrease the very high porosity of the as-coated tapes (70-80% porosity reduced to 62%) and improving the electrical contact. FE-SEM images showed the good distribution of the carbon black for the three electrodes while still having room for improvement and evidencing the high porosity, in particular for the two doped samples with spherical nanoparticles. The adhesion strength was below cell manufacturing target threshold (10N/m) for the Fe-LNMO electrode, ascribable to the less dense nanoparticles obtained via ASP synthesis (see low measured tap density, 0.7g/cm³) generating higher surface area that would require higher binder ratio than the 8:1 used in the fixed formulation in this study.

Table 2. Electrode mechanical characteristics including morphology by FE-SEM and adhesion (Peel resistance, 90° test. Standard deviation of three measured samples per electrode shown in brackets).

Electrode	LNMO/FePO ₄	Al-LNMO	Fe-LNMO
Powder Tap Density (g/cm ³)	1.4	1.3	0.7
Density as-coated (g/cm ³)	0.92	0.98	0.78
Calendered to 1.5g/cm ³ (FE-SEM surface @1000x)			
R peel (N/m)	34(1)	28(2)	9(2)

The electrochemical performance of the prepared electrodes has been analyzed by assembling and testing coin cells (CR2025, Hohsen), initially in HCC configuration using Li metal disk (50µm, Rockwood Lithium) as counter electrode. The cycle life of the prepared cathodes was investigated in FCC with graphite anode (aqueous formulation with graphite developed within the project). One layer of polyolefin Celgard 2325 separator was used in all coin cells with 1M LiPF₆ EC/EMC electrolytes (formulation optimised with an additive for high voltage operation in FCC).

Charge-discharge capability tests at different C-rates (Fig. 9, Left) revealed best performance for doped LNMOs (Fe-LNMO, 135mAh/g and Al-LNMO, 133mAh/g at C/5) whereas the FePO₄-coated LNMO showed between 10% (120mAh/g at C/5) and 20% (above 2C) lower specific capacity. The FePO₄ phase layer is likely hindering

the electrochemical activity of this active material, affecting the redox reaction centered around 4.0V, as observed on cyclic voltammetry by Kohs et al. Between the two doped samples, Al-LNMO provided higher capacity at 5C discharge ($>100\text{mAh/g}$), while Fe-LNMO recovered best from this high C-rate and retained the initial capacity in subsequent cycles, including 3C charge.

Full coin cells of these cathodes with negative graphite electrode have provided further insights towards proof-of-concept LNMO-based Li-ion battery cells (Fig. 9, Right). The initial capacity loss (ICL) analysed on the formation cycle at C/20, revealed values of ca. 21% capacity loss, which is acceptable but still to be reduced by cathode density and cell balancing optimisation (10% would be due to the SEI formation in graphite anode). Fe-LNMO cells exhibited an even higher loss (31%) that may be correlated with the higher relative porosity and surface active area of this cathode promoting further electrolyte degradation and likely a thicker cathode/electrolyte interface (solid permeable interface, SPI). Cycling test carried out at 1C rate showed the highest capacity retention for the coated LNMO/FePO₄ cathode, with up to 500 cycles at 70% capacity retention (also described as the State of Health, SOH = 70%) although initial capacity was also lowest (92mAh/g). Alternatively, doped samples provided higher initial specific discharge capacity (110mAh/g Fe-LNMO and 115mAh/g Al-LNMO) but faster decay: Al-doped cathode cells exhibited a very sharp initial drop with only 110 cycles while Fe-LNMO provided significantly better cycle life with up to 315 full cycles until 70% SOH, thus providing the best overall performance.

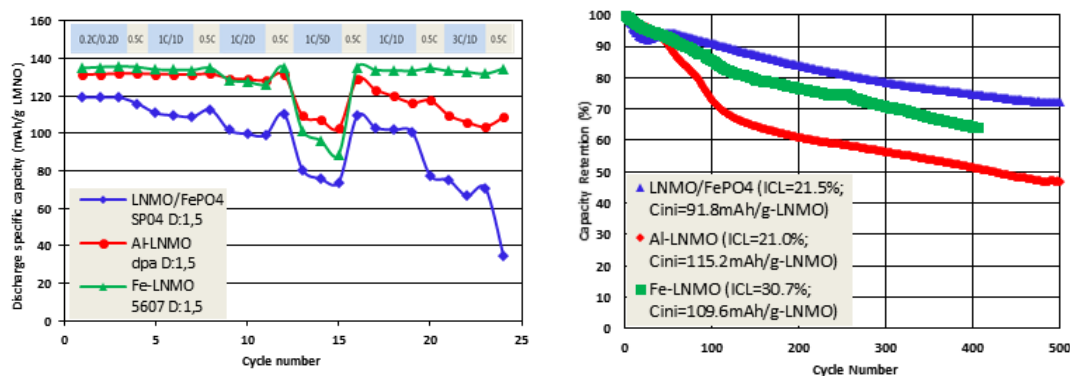


Fig. 9 Electrochemical performance of the electrodes. Left: C-rate capability test in HCC (vs. Li/Li⁺; C=130mAh/g); Voltage window [3.5-5.0V]. Right: Cycle-life at 1C rate for FCC (vs. graphite anode, Actilon2/45/CMC/SBR=94/1.5/2.5/2); Cathode loading 1.5mAh/cm²; Electrode capacity balance, a/c = 1.12-1.15; Cycled CCCV 4.8V – CC 3.6V. Temperature at 25±1°C.

5. Conclusion

A number of aerosol/liquid/solid based techniques has been employed for the realisation of high voltage cathode materials based on LNMO. Among the ones synthesised, two doped and one coated LNMO were the best performers and were presented in this work. Based on advanced synthesis technologies and subsequent calcination, various LNMO structures can be realized with main differences existing in shape (spherical or amorphous), size and structure (nano-structures with a varying degree of porosity). Apart from the obvious material characteristics such as the composition and purity, the structural features mentioned above as well as the doping and coating play a significant role in the electrode coating quality as well as the final specific energy density and cyclability. Non-spherical particles may lead to less stable slurries and perhaps smaller energy densities. More porous structures, like the ones produced by Aerosol-based technique, need more binder in the electrode formulation and are prone to higher initial capacity losses due to higher electrolyte degradation. On the other hand, they demonstrate high enough specific capacity and cycling ability. Application of a protective coating can have a significant effect on cycling ability but, as expected, lowers the material's specific energy capacity.

The attained results show that 5V cathode materials with high capacities are possible with doped LNMO structures even at high charging/discharging rates ($>130\text{mAh/g}$ at C/5 and $>100\text{mAh/g}$ at 1C in the voltage window 3.5-5V). The coated material managed a capacity retention of 70 % for up to 500 cycles at the 1C rate. However, depending on the specific application, several parameters have to be optimised with the most important ones being the electrode formulation (carbon and binder content), the electrode coating density and quality, the electrolyte and the cell balancing.

Acknowledgements

The presented work has been funded by the H2020 project eCAIMAN (reference number 653331).

References

- Amdouni, N., Zaghib, K., Gendron, F., Mauger, A., Julien, C.M., 2006. Structure and insertion properties of disordered and ordered $\text{LiNi}_{0.5}\text{Mn}_{1.5}\text{O}_4$ spinels prepared by wet chemistry, *Ionics* 12, 117–126.
- Feng, J., Huang, Z., Guo, C., Chernova, N.A., Upreti, S., Whittingham, M.S., 2013. An Organic Co-precipitation Route to Synthesize High Voltage $\text{LiNi}_{0.5}\text{Mn}_{1.5}\text{O}_4$, *Applied Materials & Interfaces* 5, 10227–10232.
- Gu, Y.J., Li, Y., Fu, Y., Zang, Q.F., Liu, H.Q., Ding, J.X., Wang, Y.M., Wang, H.F., Ni, J., 2015. $\text{LiNi}_{0.5}\text{Mn}_{1.5}\text{O}_4$ synthesized through ammonia-mediated carbonate precipitation, *Electrochimica Acta* 176, 1029–1035.
- Kim, M.G., Cho, J., 2009. Reversible and High-Capacity Nanostructured Electrode Materials for Li-Ion Batteries *Advanced Functional Materials* 19, 1497–1514.
- Kohs, W., Kahr, J., Ahniyaz, A., Zhang, N., Trifonova, A., 2017. Electrolyte-cathode interactions in 5-V lithium ion cells, *Journal of Solid State Electrochemistry*, 1–13.
- Kraytsberg, A., Ein-Eli, Y., 2012. Higher, Stronger, Better... A Review of 5 Volt Cathode Materials for Advanced Lithium-Ion Batteries, *Advanced Energy Materials* 2, 922–939.
- Lee, Y.S., Sun, Y.K., Ota, S., Miyashita, T., Yoshio, M., 2002. Preparation and characterization of nano-crystalline $\text{LiNi}_{0.5}\text{Mn}_{1.5}\text{O}_4$ for 5 V cathode material by composite carbonate process, *Electrochemical Communications* 4, 989–994.
- Lin, H.B., Zhang, Y.M., Rong, H.B., Mai, S.W., Hu, J.N., Liao, Y.H., Xing, L.D., Xu, M.Q., Li, X.P., Li, W.S., 2014. Crystallographic facet- and size-controllable synthesis of spinel $\text{LiNi}_{0.5}\text{Mn}_{1.5}\text{O}_4$ with excellent cyclic stability as cathode of high voltage lithium ion battery, *Journal of Materials Chemistry A* 2, 11987–11995.
- Liu, D., Zhu, W., Trottier, J., Gagnon, F., Julien, C.M., Goodenough, J.B., Zaghib, K., 2014. Spinel materials for high-voltage cathodes in Li-ion batteries, *RSC Advances* 4, 154–167.
- Liu, G., Kong, X., Sun, H., Wang, B., 2014. Extremely rapid synthesis of disordered $\text{LiNi}_{0.5}\text{Mn}_{1.5}\text{O}_4$ with excellent electrochemical performance, *Ceramics International* 40, 14391–14395.
- Lorentzou, S., Kastrinaki, G., Pagkoura, C., Konstandopoulos, A.G., 2011. Oxide Nanoparticles for Hydrogen Production from Water-Splitting and Catalytic Oxidation of Diesel Exhaust Emissions, *Nanoscience and Nanotechnology Letters* 3, 697–704.
- Lorentzou, S., Pagkoura, C., Zygogianni, A., Kastrinaki, G., Konstandopoulos, A.G., 2009. Catalytic Nano-structured Materials for Next Generation Diesel Particulate Filters, *SAE International Journal of Materials and Manufacturing* 1, 189–198.
- Lorentzou, S., Zygogianni, A., Tousimi, K., Agrafiotis, C., Konstandopoulos, A.G., 2009. *Journal of Alloys and Compounds* 483, 302–305.
- Miao, C., Bai, P.F., Jiang, Q.Q., Wang, X.Y., 2014. A novel synthesis and characterization of LiFePO_4 and LiFePO_4/C as a cathode material for lithium-ion battery, *Journal of Power Sources* 246, 232–238.
- Myung, S.-T., Amine, K., Sun, Y.-K., 2015. Nanostructured cathode materials for rechargeable lithium batteries, *Journal of Power Sources* 283, 219–236.
- Myung, S.T., Komada, S., Kumagai, N., Yashiro, H., Chung, H.T., Cho, T.H., 2002. Nano-crystalline $\text{LiNi}_{0.5}\text{Mn}_{1.5}\text{O}_4$ synthesized by emulsion drying method, *Electrochimica Acta* 47, 2543–2549.
- Oh, S.H., Chung, K.Y., Jeon, S.H., Kim, C.S., Cho, B.W., 2009. Structural and electrochemical investigations on the $\text{LiNi}_{0.5-x}\text{Mn}_{1.5-x}\text{M}_{x+0.5}\text{O}_4$ ($M = \text{Cr}, \text{Al}, \text{Zr}$) compound for 5V cathode material, *Journal of Alloys and Compounds* 469, 244–250.
- Pasero, D., Reeves, N., Pralong, V., West, A., 2008. Oxygen Nonstoichiometry and Phase Transitions in $\text{LiMn}_{1.5}\text{Ni}_{0.5}\text{O}_{4-\delta}$, *J. Electrochemical Society* 155, A282–A291.
- Patoux, S., Daniel, L., Bourbon, C., Pagano, C., Jouanneau, S., Martinet, S., 2009. High voltage spinel oxides for Li-ion batteries: From the material research to the application, *Journal of Power Sources* 189, 344–352.
- Pieczonka, N.P.W., Liu, Z., Lu, P., Olson, K.L., Moote, J., Kim, J.-H., 2013. Understanding Transition-Metal Dissolution Behavior in $\text{LiNi}_{0.5}\text{Mn}_{1.5}\text{O}_4$ High-Voltage Spinel for Lithium Ion Batteries, *Journal of Physical Chemistry C* 117, 15947–15957.
- Potapenko, A.V., Kirillov, S.A., 2014. Lithium manganese spinel materials for high-rate electrochemical applications, *Journal of Energy Chemistry* 23, 543–558.
- Reddy, T.B., Linden, D., 2011. *Linden's Handbook of Batteries* (4th ed.), McGraw-Hill, New York.
- Song, J., Shin, D.W., Lu, Y., Amos, C.D., Manthiram, A., Goodenough, J.B., 2012. Role of Oxygen Vacancies on the Performance of $\text{Li}[\text{Ni}_{0.5-x}\text{Mn}_{1.5+x}]\text{O}_4$ ($x = 0, 0.05$, and 0.08) Spinel Cathodes for Lithium-Ion Batteries, *Chemistry of Materials* 24, 3101–3109.
- Takahashi, K., Saitoh, M., Sano, M., Fujita, M., Kifune, K., 2004. Electrochemical and Structural Properties of a 4.7 V-Class $\text{LiNi}_{0.5}\text{Mn}_{1.5}\text{O}_4$ Positive Electrode Material Prepared with a Self-Reaction Method, *Journal of Electrochemical Society* 151, 173.
- Wang, H., 2015. $\text{LiNi}_{0.5}\text{Mn}_{1.5}\text{O}_4$ Cathodes for Lithium Ion Batteries: A Review, *Journal of Nanoscience & Nanotechnology* 15, 6883–6890.
- Wang, L., Chen, D., Wang, J., Liu, G., Wu, W., Liang, G., 2016. Synthesis of $\text{LiNi}_{0.5}\text{Mn}_{1.5}\text{O}_4$ cathode material with improved electrochemical performances through a modified solid-state method, *Powder Technology* 292, 203–209.
- Wen, L., Lu, Q., Xu, G., 2006. Molten salt synthesis of spherical $\text{LiNi}_{0.5}\text{Mn}_{1.5}\text{O}_4$ cathode materials, *Electrochimica Acta* 51, 4388–4392.
- Xu, X.L., Deng, S.X., Wang, H., Liu, J.B., Yan, H., 2017. Research Progress in Improving the Cycling Stability of High Voltage $\text{LiNi}_{0.5}\text{Mn}_{1.5}\text{O}_4$ Cathode in Lithium Ion Battery, *Nano-Micro Letters* 9:22.
- Xue, Y., Wang, Z., Yu, F., Zhang, Y., Yin, G., 2014. Ethanol-assisted hydrothermal synthesis of $\text{LiNi}_{0.5}\text{Mn}_{1.5}\text{O}_4$ with excellent long-term cyclability at high rate for lithium-ion batteries, *Journal of Materials Chemistry A* 2, 4185–4191.
- Yi, T.-F., Mei, J., Zhu, Y.-R., 2016. Key strategies for enhancing the cycling stability and rate capacity of $\text{LiNi}_{0.5}\text{Mn}_{1.5}\text{O}_4$ as high-voltage cathode materials for high power lithium-ion batteries, *Journal of Power Sources* 316, 85–105.
- Zheng, J., Xiao, J., Yu, X., Kovarik, L., Gu, M., Omenya, F., Chen, X., Yang, X.Q., Liu, J., Graff, G.L., Whittingham, M.S., Zhang, J.G., 2012. Enhanced Li^+ ion transport in $\text{LiNi}_{0.5}\text{Mn}_{1.5}\text{O}_4$ through control of site disorder, *Physical Chemistry Chemical Physics* 14, 13515–13521.
- Zhu, Z., Yan, H., Zhang, D., Li, W., Lu, Q., 2013. Preparation of 4.7 V cathode material $\text{LiNi}_{0.5}\text{Mn}_{1.5}\text{O}_4$ by an oxalic acid-pretreated solid-state method for lithium-ion secondary battery, *Journal of Power Sources* 224, 13–19.